Half-Sine Wave Modulation Technique a New Method for Generating Variable Frequency Sinusoidal Current

Sharifaddin Sharif

***Abstract*—In this paper, a new method for generating variable-frequency sinusoidal current is proposed. This method is based on the series resonant inverter and can be used in adjustable frequency drives. In the proposed method, each half-cycle of the fundamental frequency consists of a number of half-sine waves with different amplitudes and widths, which are arranged side-by-side. In this method, switching losses and output harmonic content can be significantly reduced. The circuit needed to generate this waveform can be implemented by a modified series resonant inverter with a number of capacitors. A performance comparison of the proposed method and the conventional sinusoidal pulsewidth modulation technique is presented to evaluate improvements in the method.**

***Index Terms*—Series resonant inverter, sinusoidal pulsewidth modulation (SPWM), variable frequency drive.**

I. Introduction

SINE wave inverters with the ability to control output amplitude, frequency, and phase are very important in industry, office, and home appliances. Examples of these applications are renewable energy sources, uninterruptible power supplies, adjustable speed drives (ASDs), etc.

The output of an ideal inverter is expected to be a perfect sinusoidal waveform without harmonic. Many methods have been developed to achieve this goal. The use of any of these methods depends on the power range, the allowable loss, the load sensitivity to the harmonics, and the cost.

The pulsewidth modulation (PWM) technique is very popular for generating sinusoidal output in converters and has been discussed extensively in the literature [1]–[3].

A disadvantage of PWM converters is that PWM rectangular waveforms produce many harmonics and switching loss in semiconductor devices, which limit the application of the converters. Rectangular waveforms also inherently generate electromagnetic interference (EMI) [3], [4].

A review of the literature indicates that a number of strategies have been developed to improve the performance and the quality

Manuscript received March 27, 2018; revised June 12, 2018 and August 21, 2018; accepted October 15, 2018. Date of publication October 21, 2018; date of current version May 2, 2019. This work was supported by the Islamic Azad University, Kazerun Branch, Kazerun, Iran. Recommended for publication by Associate Editor D. G. Xu.

The author is with the Department of Electrical Engineering, Kazerun Branch, Islamic Azad University, Kazerun 73198-66451, Iran (e-mail:

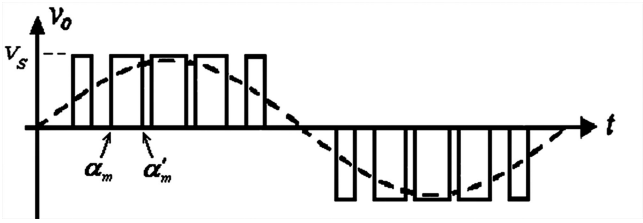

Fig. 1. Traditional SPWM technique. Unipolar switching scheme with five pulses per half-cycle.

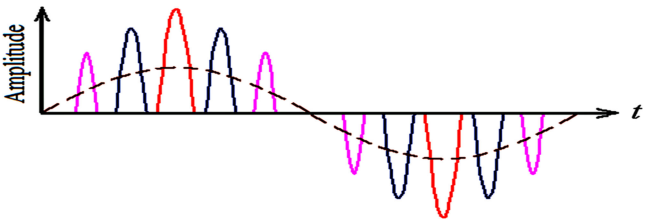

Fig. 2. Proposed method for producing a sinusoidal output waveform.

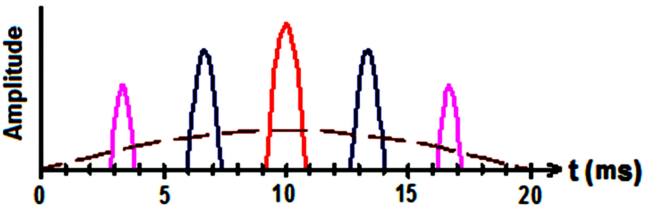

Fig. 3. If the half-sine pulses are far from each other, the period of the fundamental harmonic increases and the frequency decreases.

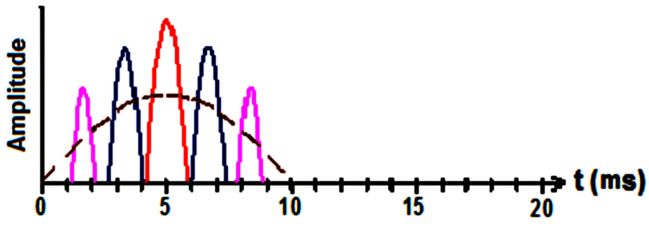

Fig. 4. If the half-sine pulses are close to each other, the period of the fundamental harmonic decreases and the frequency increases.

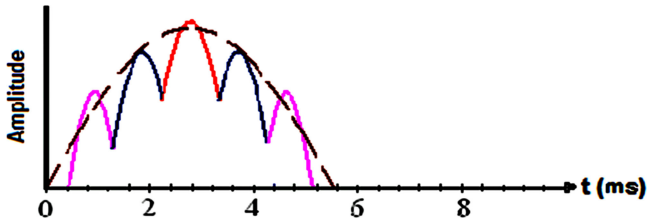

Fig. 5. Half-sine pulses can overlap each other to produce a higher output frequency.

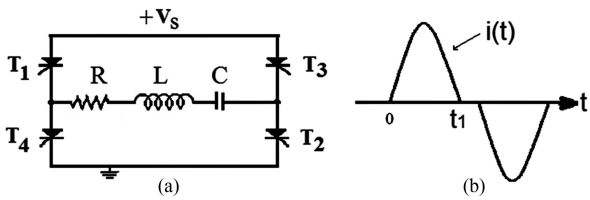

Fig. 6. (a) Circuit diagram of a thyristor based series resonant inverter. (b) Current waveform through the circuit.

shown in the form of the following equation:

$$B_n = \sum_{m=1}^{p} \frac{2V_S}{n\pi}(\cos n\alpha_m - \cos n\alpha'_m) \tag{1}$$

for $n = 1, 3, 5, 7, \ldots$ where B_n is the amplitude of the nth harmonic, p is the number of pulses per half-cycle, V_S is the amplitude of the pulses, and α_m and α'_m are the start and the end point of mth pulse, respectively.

B. Description of the Proposed Method

Fig. 2 shows the proposed method for producing a sinusoidal output waveform.

As can be seen, each half-cycle of the fundamental frequency, consist of a number of half-sine pulses with different amplitude and width, which are arranged side-by-side. The largest half-sine pulse is located at the midpoint, and the other small halves are symmetrically located on both sides.

This method is almost similar to the SPWM, except that instead of rectangular pulses with constant amplitudes, semi-sinusoidal pulses are used with different amplitudes. Obviously, the resultant of these pulses are closer to a sinusoidal wave and have fewer harmonics.

Changing frequency is very simple. If the half-sine pulses are far from each other, the period of the fundamental harmonic increases (see Fig. 3). On the other hand, if the half-sine pulses are close to each other, the period of the fundamental harmonic decreases (see Fig. 4). To produce a higher output frequency, the half-sine pulses can overlap each other as shown in Fig. 5. The fundamental component of the waves is also shown in the figures by the dashed line.

III. Generating the Half-Sine Pulses

In order to generate half-sine pulses and implementation of the half-sine modulation, a circuit based on a series resonant inverter is used. Therefore, first, a review of a simple series resonant inverter is provided.

A. Conventional Series Resonant Inverter

Series resonant inverter topology is a familiar circuit in the field of power electronics. They have been widely applied to dc–dc converters, photovoltaic power conversion system, battery chargers [27]–[35], and induction heating.

A circuit diagram of a thyristor-based series resonant inverter is shown in Fig. 6. The switches are driven by non-overlapping gating signals with a small dead time at the operating frequency. The series resonant circuit formed by L, C, and R must be underdamped [1].

When thyristors T_1 and T_2 are fired, a positive resonant pulse of current flows through the load and the current falls to zero at time t_1, then T_1 and T_2 are self-commutated. Firing of thyristors

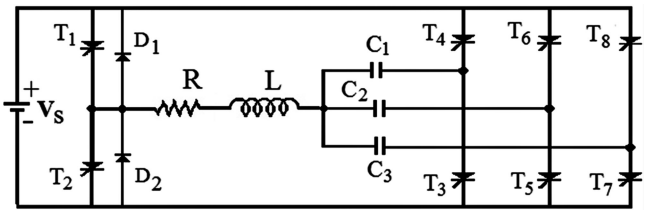

Fig. 7. Circuit diagram of the proposed multi-capacitor series resonant inverter (MCSRI) with three capacitors for three half-sine pulses per half-cycle.

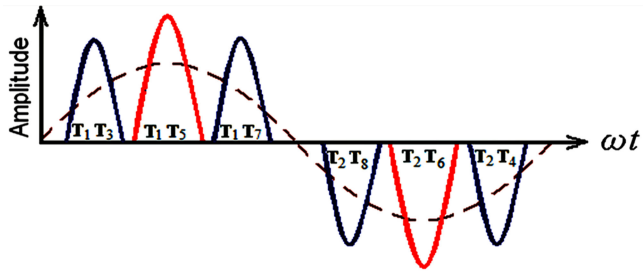

Fig. 8. Output waveform of MCSRI with three capacitors in the circuit.

T_3 and T_4, generates a negative resonant current through the load and T_3 and T_4 are also self-commutated. Sequential triggering of thyristors generates a current similar to the sinusoidal waveform in the circuit. The instantaneous load current is described by the following equations and can be found in detail in [1]:

$$i(t) = \frac{V_1}{\omega_r L} e^{-\alpha t} \sin \omega_r t \tag{2}$$

where ω_r is a resonant frequency

$$\omega_r = \left(\frac{1}{LC} - \frac{R^2}{4L^2} \right)^{1/2} \tag{3}$$

and

$$V_1 = \frac{V_S e^z}{e^z} - 1 \tag{4}$$

$$\text{where } z = \alpha\pi/\omega_r \text{ and } \alpha = R/2L. \tag{5}$$

B. Design and Description of the Proposed Circuit for Implementing the HSWM Technique

Fig. 7 shows the circuit diagram of the proposed inverter for generating the half-sine waves. It is a modified circuit of the conventional thyristor base series resonant inverter with additional capacitor and switches. Because of the number of capacitors, it can be called MCSRI.

The circuit diagram in Fig. 7 is designed with three capacitors for three half-sine pulses per half-cycle. By providing $C_1 = C_3$ and $C_2 > C_1$ and C_3, the waveforms of the HSWM can be generated. The switching scheme for generating the positive half-sine pulses are T_1T_3–T_1T_5–T_1T_7 and for generating the negative half-sine pulses are T_2T_8–T_2T_6–T_2T_4.

D_1 and D_2 are freewheeling diodes. Note that the other thyristors do not require anti-parallel diodes because they create new paths that the capacitors voltage are disturbed.

The generated waveform when three capacitors are in the circuit is shown in Fig. 8. As mentioned earlier, by increasing or decreasing the interval between the triggering of the switches, the frequency of the fundamental output component can be changed.

In an underdamped circuit, by neglecting R, the width of each half-sine pulse is $\pi\sqrt{LC_m}$ and the amplitude of each half-sine pulse is $V_S\sqrt{\frac{C_m}{L}}$, where C_m is the corresponding capacitor [1].

The output harmonic content is reduced by increasing the number of half-sine pulses per half-cycle. For this purpose, the number of capacitors and the number of thyristor arms should be increased. Obviously, there must be a compromise between the number of pulses and the output harmonic content.

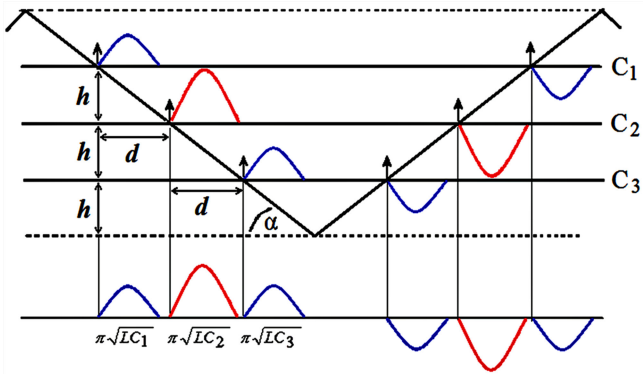

Fig. 9. Cross location of each parallel line with the triangle legs, determine the trigger time of the switches (or the start of each half-sine pulse). Varying α or h can determine the interval between half-sine pulses.

The algorithm for generating the gating signals is similar to that of SPWM except that, instead of the sinusoidal control signal, several equidistant parallel lines (equal to the number of capacitors) are used. As shown in Fig. 9, each line corresponds to one capacitor. The cross location of each parallel line with the triangle legs, determine the trigger time of the switches (or the start of each half-sine pulse). The middle line corresponds to the C_2 and the upper and lower lines correspond to the C_1 and C_3, respectively.

As can be observed in Fig. 9, α (the angle between the horizontal parallel lines and the triangle legs), or h (the distance between parallel lines), can determine the interval between the half-sine pulses (d). If α gets smaller, or, if parallel lines get farther apart, the interval between the half-sine pulses will be greater and vice versa.

Since the relation between α and its tangent is highly nonlinear, it is preferred to fix α and change h.

By fixing $\alpha = 45°$, when the parallel lines are closing to each other, the interval between the half-sine pulses will be smaller. The minimum value of h is corresponding to a state in which the half-sine pulses due to C_1 and C_3 lie together. This situation shows in Fig. 10. The minimum of h and d, are shown by $h_{\min}$ and $d_{\min}$, respectively.

It is notable that the waves due to C_1 and C_3 must not overlap each other. Because this means that the two thyristors are simultaneously triggered in an arm, which leads to a power supply short circuit.

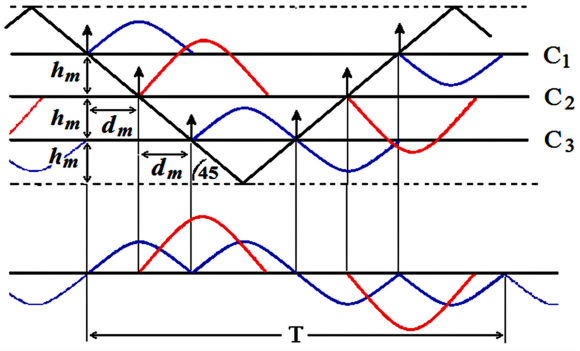

Fig. 10. Minimum value of h is corresponding to a state in which half-sine pulses due to C_1 and C_3 lie together ($m = 1$).

In this case, regarding $\alpha = 45°$

$$h_{\min} = d_{\min}. \tag{6}$$

Note that the $d_{\min}$ is equal to the half-duration of the half-sine pulse due to C_1 (or C_3). Then

$$h_{\min} = d_{\min} = \frac{1}{2}\pi\sqrt{LC_1}. \tag{7}$$

It can be seen in Fig. 10 that a fundamental output period at maximum frequency is equivalent to eight times the distance between parallel lines or equal to the four times the half-period corresponding to the resonant of C_1 (or C_3). Thus, the capacitance of C_1 determines the maximum output frequency

$$T_{\min} = \frac{1}{f_{\max}} = 8h_{\min} = 4\pi\sqrt{LC_1} \tag{8}$$

where $T_{\min}$ is the period and $f_{\max}$ is the maximum output frequency.

The modulation index (m) can be defined as follows:

$$m = \frac{h_{\min}}{h}. \tag{9}$$

By this definition, $m = 1$ is a case in which the distance between the parallel lines is minimal.

When the parallel lines move away from each other, as shown in Fig. 9 ($m < 1$), the interval between the half-sine pulses will also be greater. In all the cases

$$h = d = \frac{h_{\min}}{m} \tag{10}$$

$$T = 8d = 8h = 8\frac{h_{\min}}{m} \tag{11}$$

$$f = \frac{1}{T} = \frac{m}{8h_{\min}} = mf_{\max} \tag{12}$$

where T is the period and f is the fundamental frequency of output current.

IV. Harmonic Analysis of the HSWM Waveform

In order to compute the harmonic content of HSWM waveform, we assume P as the number of half-sine pulses per half-cycle. Note that the waveform has an odd and half-wave symmetry. The general form of a Fourier series of an odd function is as follows:

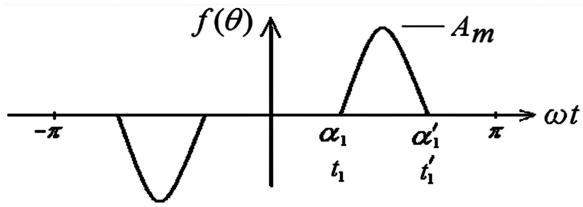

Fig. 11. One pair of the half-sine pulses in a period of fundamental frequency.

$$i(t) = \sum_{n=1,3,5,\ldots}^{\infty} B_n \sin n\omega t \tag{13}$$

where B_n is the amplitude of the nth harmonic. B_n can be determined by considering a pair of pulses in one period, and compute the Fourier coefficient for these pairs; and then, the effects of all pulses can be combined together. Fig. 11 shows a pair of half-sine pulses in a period of the fundamental frequency. If the positive half-sine pulse of the mth pair, starts at $\omega t_1 = \alpha_1$ and ends at $\omega t'_1 = \alpha'_1$, the Fourier coefficient for a pair of pulses (b_n) is

$$b_n = \frac{2}{\pi}\int_{\alpha_1}^{\alpha'_1} f(\theta)\sin n\theta d\theta. \tag{14}$$

According to Fig. 11, $f(\theta)$ is equal to

$$f(\theta) = A_m \sin\frac{\omega_m}{\omega}(\theta - \alpha_1) \tag{15}$$

where A_m is the amplitude and ω_m is the angular frequency of the mth half-sine pulse.

By substituting (15) in (14), yields

$$b_n = \frac{2}{\pi}\int_{\alpha_1}^{\alpha'_1} A_m \sin\frac{\omega_m}{\omega}(\theta - \alpha_1)\sin n\theta d\theta. \tag{16}$$

In Fig. 11, we have $t'_1 - t_1 = \frac{(\alpha'_1 - \alpha_1)}{\omega} = \pi\sqrt{LC_m}$ and in a resonant inverter in underdamped condition $\omega_m \approx \frac{1}{\sqrt{LC_m}}$. Hence, it results in that: $\frac{\omega_m}{\omega}(\alpha'_1 - \alpha_1) = \pi$.

Given this relation and simple algebraic manipulation, the Fourier coefficient is obtained for a pair of sine pulses as follows:

$$b_n = \frac{1}{\pi}A_m\left[\frac{2(\frac{\omega_m}{\omega})}{(\frac{\omega_m}{\omega})^2 - n^2}(\sin n\alpha_1 + \sin n\alpha'_1)\right]. \tag{17}$$

The coefficient B_n in (13) (i.e., the amplitude of the nth harmonic) can be obtained by combining the effects of all sine pulses

$$B_n = \frac{1}{\pi}\sum_{m=1}^{p} A_m\left[\frac{2(\frac{\omega_m}{\omega})}{(\frac{\omega_m}{\omega})^2 - n^2}(\sin n\alpha_m + \sin n\alpha'_m)\right] \tag{18}$$

for $n = 1, 3, 5, 7, \ldots$ where p is the number of half-sine pulses per half-cycle.

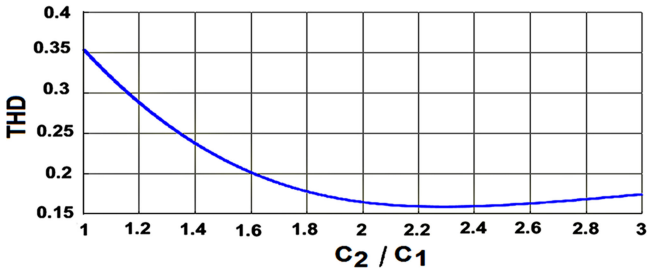

Fig. 12. THD versus C_2/C_1 in three-pulse mode HSWM technique.

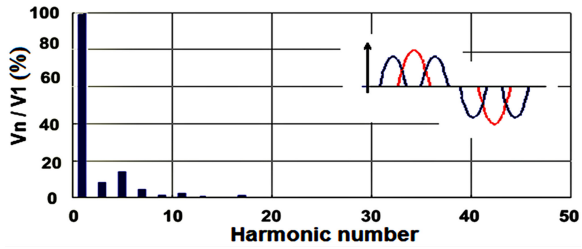

Fig. 13. HSWM harmonic spectrum for three half-sine pulses per half-cycle for $m = 0.83$, fundamental frequency 50 Hz and THD = 18.5%.

V. Comparing the Harmonic Spectrum of SPWM With the Proposed HSWM Technique

The minimum number of pulses per half-cycle in the SPWM technique is three. Therefore, it might be a good idea to compare the SPWM technique with the proposed HSWM technique in terms of the total harmonic distortion (THD) in three pulses per half-cycle and for 60-Hz maximum output frequency. This comparison can be generalized to waveforms with more pulses and reveals some aspects of the HSWM.

For three-pulse mode, three capacitors are needed. Then, first of all, the capacitance of C_1, C_2, and C_3 must be computed.

It should be noted that C_1 and C_3 ($C_1 = C_3$) determine the amplitude and duration of the lateral sine pulses. From (8)

$$T_{\min} = 4\pi\sqrt{LC_1}. \tag{19}$$

$T_{\min} = 1/60$ ms and if $L = 32$ mH then from (19) the result is $C_1 = C_3 = 55$ μF.

To compute C_2 (which determines the amplitude and duration of the central sine pulse), it is noteworthy that its capacitance should be such that the amplitude of fundamental output harmonic should be maximized and the other harmonics amplitude should be minimized. In other words, the THD should be minimized.

If assuming the capacitance of C_1 ($C_3 = C_1$) as the base, by computing the THD in terms of the ratio of C_2/C_1, the result as shown in Fig. 12 shows that the best ratio for minimum output harmonic distortion is 2.2–2.4.

That is, in three-pulse mode HSWM technique in order to have the lowest THD, the capacitance of the C_2 must be 2.2–2.4 times the C_1 capacitance. Hence

$$C_2 = 2.2C_1 \text{ then } C_2 = 121\ \mu\text{F}.$$

The harmonic spectrum of an HSWM waveform with three half-sine pulses per half-cycle for $m = 0.83$ and the harmonic spectrum of a unipolar SPWM waveform for three pulses per half-cycle for $m = 0.8$ are shown in Figs. 13 and 14, respectively.

MATLAB fast Fourier transform analysis (FFT) was used to evaluate these harmonic spectrums. The first 50 harmonics were used for the THD calculation. Equations (1) and (18) can also be used to obtain these harmonic spectrums.

The bar diagrams in Fig. 13 shows that in the HSWM technique, the THD is significantly reduced compared with that of SPWM which is shown in Fig. 14. Reducing THD from 70.8% in SPWM to 18.5% in the HSWM is very valuable.

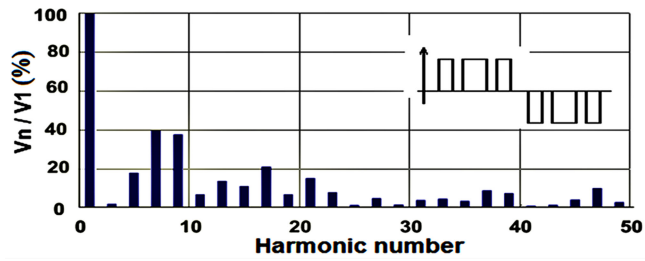

Fig. 14. SPWM harmonic spectrum for three pulses per half-cycle for $m = 0.8$, fundamental frequency 50 Hz and THD = 70.8%.

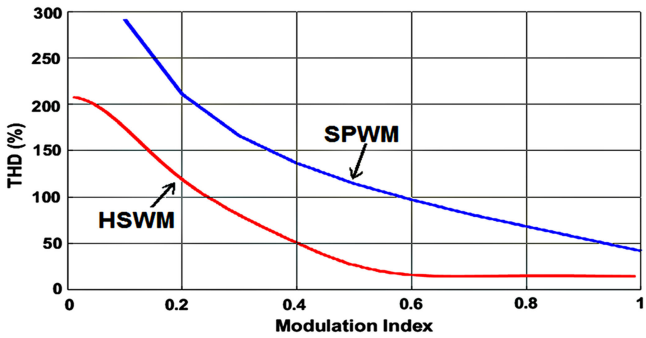

Fig. 15. Comparison of THD versus modulation index in two HSWM and SPWM techniques in three pulses per half-cycle.

Comparison of the two figures also shows that in the HSWM technique, higher order harmonics are completely attenuated. Nearly, after the 19th harmonic, there are no high-frequency harmonics in the HSWM technique in a three pulse per half-cycle.

Generally, this type of modulation eliminates all high-frequency harmonics. In other words, in the HSWM technique, there is no EMI problem.

Graph of the THD versus the modulation index, in two HSWM and SPWM techniques, is shown in Fig. 15. As can be seen, for the entire domain of the modulation index, the THD in the HSWM technique is much lower compared to the conventional SPWM.

Similar the SPWM, in the HSWM technique, there is also a linear relationship between the peak fundamental output and the modulation index for $m < 1$. In other words, the amplitude variation of the fundamental output component is linear with respect to the modulation index; which, is a desirable feature, especially in ac motor control. Fig. 16 shows this relationship.

Fig. 16. Amplitude variation of the output fundamental component with respect to modulation index in HSWM technique.

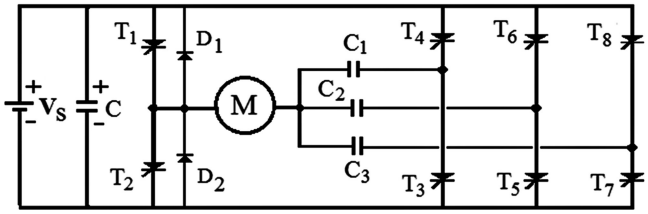

Fig. 17. Experimental circuit for HSWM technique in three-pulse mode.

Similar results are obtained by comparing the SPWM with the HSWM technique for more pulses in a half-cycle.

VI. Experimental Results

The HSWM technique was checked by experimental tests. The experimental setup, as shown in Fig. 17, used BT151 thyristors as switches. Normally, the thyristors require dv/dt protection and isolated drive circuits. The capacitor C is a 1000-μF electrolytic capacitor parallel with supply to reduce the current ripple caused by the resonant pulses.

A 110-V, 50-Hz, 1-A, 3000-r/min single phase induction motor has been used as a load, which was replaced instead R and L in the circuit of Fig. 7. In fact, the resistance of stator winding is used instead of the resistor R and the transient inductance of the motor is used instead of the resonant inductance L in Fig. 7. The stator resistance of the test motor was 3.4 Ω and the inductance was 32 mH.

The motor current is measured by the voltage drop across a 0.1-Ω series resistance and waveforms are captured by an analog oscilloscope.

For three-pulse mode, as explained in Section V, $C_1 = C_3 =$ 50 microfarad and $C_3 = 120$ microfarad was chosen. According to (19), with the values of $L = 32$ mH and $C_1 = 50$ μF, the maximum output frequency would be about 63 Hz.

The gating signals for controlling the interval between pulses were generated by an ATMEGA32 microcontroller, operating with 8-MHz clock frequency, based on the described method in Section III-B.

By changing the time interval between triggering the switches, the frequency was changed and the motor speed could be controlled.

Figs. 18 and 19 show steady-state waveforms of the motor current in three-pulse mode, in two cases: 25-Hz frequency with

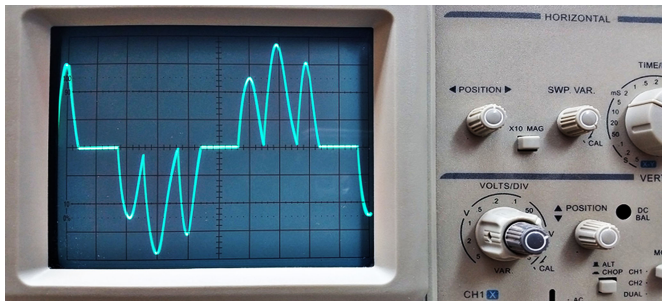

Fig. 18. Experimental output waveform of inverter (motor current) in a three-pulse mode at frequency of 25 Hz, (Tim/Div = 5 ms).

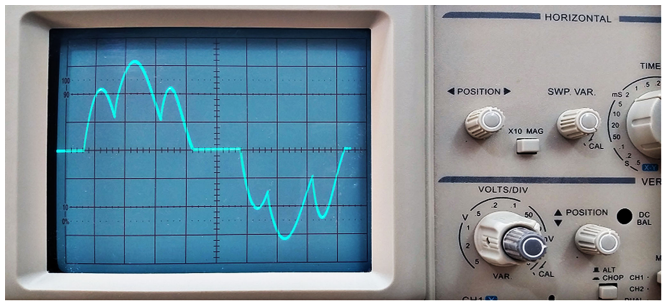

Fig. 19. Experimental output waveform of inverter (motor current) in a three-pulse mode at frequency of 50 Hz, (Tim/Div = 2 ms).

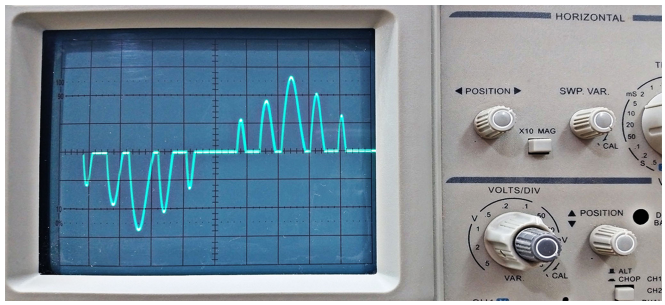

Fig. 20. Experimental output waveform of inverter (motor current) in a five-pulse mode at frequency of 20 Hz (Tim/Div = 5 ms).

modulation index of 0.4 when the half-sine pulses are apart from each other, and 50-Hz frequency with modulation index of 0.8, when the half-sine pulses are overlapping.

At low frequencies, where sinusoidal pulses were far from each other, the motor worked with vibration that was something to expect. Therefore, for low-speed applications, the number of pulses in half a cycle should be increased.

As another test, for a five-pulse mode, (by adding two capacitors and two thyristor arms to the circuit of Fig. 17. The detailed analysis for selecting the capacitor is out of the scope of the present paper and is left for further.) $C_1 = C_5 = 6.3$ and $C_2 = C_4 = 20$ microfarad and $C_3 = 50$ microfarad was chosen.

Figs. 20 and 21 also show experimental results of the instantaneous current of the motor, in five-pulse mode, at 20 Hz and 50 Hz, respectively.

By using the spectrum analyzer or transmitting the current waveform to the MATLAB environment, it could be checked the

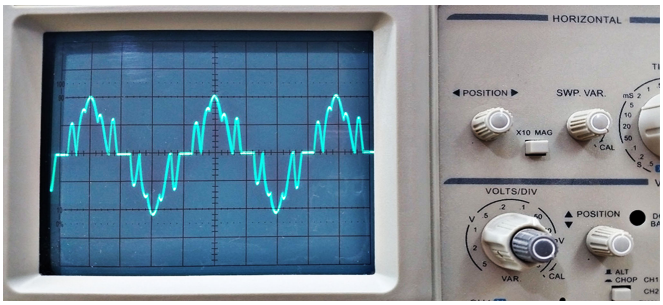

Fig. 21. Experimental output waveform of inverter (motor current) in a five-pulse mode at frequency of 50 Hz (Tim/Div = 5 ms).

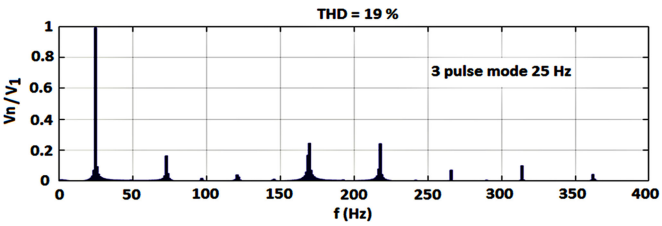

Fig. 22. Frequency spectrum of the motor current in a three-pulse mode at frequency of 25 Hz (related to Fig. 18).

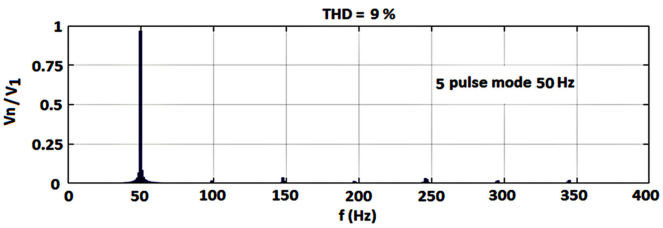

Fig. 23. Frequency spectrum of the motor current in a five-pulse mode at frequency of 50 Hz (related to Fig. 21).

frequency spectrum and harmonics of motor current practically. Figs. 22 and 23, which were obtained by sampling the motor current in the MATLAB environment and using the "FFT" and "THD" commands, show the frequency spectrum and THD of the motor current in a three-pulse mode at frequency of 25 Hz (related to Fig. 18) and in a five-pulse mode at frequency of 50 Hz (related to Fig. 21), respectively.

The frequency spectrums are revealed that the low-order harmonics can also be reduced efficiently by using more pulses (for instance 7–15 pulse) in a half-cycle.

VII. Advantage and Disadvantage of HSWM

A. Advantages

1) The circuit structure and control strategy are simple.
2) The generation of triggering pulses is very easy because they are just a time interval and can be implemented by a conventional microcontroller.
3) The thyristors in the inverter turn ON and OFF only once per cycle of the load current. In addition, because of the resonance performance, the switching losses are negligible.
4) High-frequency harmonics are reduced very fast and there is no EMI problem.
5) THD is reduced significantly with respect to the standard SPWM method.
6) The amplitude of the fundamental component is linear with respect to the modulation index. It is a desirable feature, especially in the *v/f* control method, which is the most commonly used method for ASD.

B. Disadvantage

1) Due to a resonant characteristic of the inverter, the pulses width and amplitude depend on the load parameter. Therefore, in motor speed control applications, the switching frequency may not be set to any value.
2) The frequency and amplitude of output voltage both vary whit modulation index.
3) It requires more capacitors and switches (n capacitors and $2n + 2$ switches for n pulses per half-cycle).

VIII. Conclusion

The main objective of this paper is to propose a new method for generating a variable frequency sinusoidal current. The proposed method surely has advantages and limitations.

However, the analysis indicates major improvements in the THD of the proposed scheme over a standard SPWM scheme in both low- and high-modulation indices. The major advantage of the HSWM technique over the PWM technique is that in the HSWM technique the half-sine pulses can overlap each other, Whereas, in the PWM technique, overlapping pulses (over modulation), lead to widening the center pulse and produce more harmonics.

HSWM method should not be considered a general technique for all loads. But because of the resonance nature and dependence on the load characteristics, it is suitable for devices that have an electric motor with their own drive, such as refrigerators, washing machines and dishwashers, turning machines, air conditioners, compressors, etc.

References

[1] M. H. Rashid, *Power Electronics: Circuits, Devices, and Applications*, 3rd ed. Englewood Cliffs, NJ, USA: Prentice-Hall, 2004, ch. 6.
[2] N. Mohan, T. Undeland, and W. Robbins, *Power Electronics, Converters, Applications, and Design*, 2nd ed. New York, NY, USA: Wiley, ch. 8.
[3] M. H. Rashid *Power Electronics Handbook*, 3rd ed. New York, NY, USA: Academic, 2001.
[4] P. K. Chaturvedi, S. Jain, and P. Agarwal, "Reduced switching loss pulse width modulation technique for three-level diode clamped inverter," *IET Power Electron.*, vol. 4, no. 4, pp. 393–399, Apr. 2011.
[5] J. R. Wells, X. Geng, P. L. Chapman, P. T. Krein, and B. M. Nee, "Modulation-based harmonic elimination," *IEEE Trans. Power Electron.*, vol. 22, no. 1, pp. 336–340, Jan. 2007.
[6] K. Selvajyothi and P. A. Janakiraman, "Reduction of voltage harmonics in single phase inverters using composite observers," *IEEE Trans. Power Del.*, vol. 25, no. 2, pp. 1045–1057, Apr. 2010.
[7] H. Li and R. S. Curiac, "Designing more efficient large industrial induction motors by utilizing the advantages of adjustable-speed drives," *IEEE Trans. Ind. Appl.*, vol. 46, no. 5, pp. 1805–1809, Sep./Oct. 2010.
[8] B. Zahedi and S. Vaez-Zadeh, "Efficiency optimization control of single-phase induction motor drives," *IEEE Trans. Power Electron.*, vol. 24, no. 4, pp. 1062–1071, Apr. 2009.

[9] F. Vargas-Merino, M. J. Meco-Gutiérrez, J. R. Heredia-Larrubia, and A. Ruiz-Gonzalez, "Low switching PWM strategy using a carrier wave regulated by the slope of a trapezoidal modulator wave," *IEEE Trans. Ind. Electron.*, vol. 56, no. 6, pp. 2270–2274, Jun. 2009.
[10] D. M. Divan, "The resonant DC link converter—A new concept in static power conversion," *IEEE Trans. Ind. Appl.*, vol. 25, no. 2, pp. 317–325, Mar./Apr. 1989.
[11] D. M. Divan and G. Skibinski, "Zero-switching-loss inverters for high power applications," *IEEE Trans. Ind. Appl.*, vol. 25, no. 4, pp. 634–643, Jul./Aug. 1989.
[12] J.-S. Lai and K Bose, "An induction motor drive using an improved high frequency resonant dc link inverter," *IEEE Trans. Power Electron.*, vol. 6, no. 3, pp. 504–513, Jul. 1991.
[13] J. S. Lai and F. Z. Peng, "Multilevel converters—A new breed of power converters," *IEEE Trans. Ind. Appl.*, vol. 32, no. 3, pp. 509–517, May/Jun. 1996.
[14] L. Tolbert and T. Habetler, "Novel multilevel inverter carrier-based PWM method," *IEEE Trans. Ind. Appl.*, vol. 35, no. 5, pp. 1098–1107, Sep./Oct. 1999.
[15] C.-H. Hsieh, T. J. Liang, S. Ming Chen, and S.-W. Tsai, "Design and implementation of a novel multilevel DC-AC inverter," *IEEE Trans. Ind. Appl.*, vol. 52, no. 3, pp. 2436–2443, May/Jun. 2016.
[16] M. Aleenejad, H. Mahmoudi, and R. Ahmadi, "Multifault tolerance strategy for three-phase multilevel converters based on a half-wave symmetrical selective harmonic elimination technique," *IEEE Trans. Power Electron.*, vol. 32, no. 10, pp. 7980–798, Oct. 2017.
[17] M. Aleenejad, H. Mahmoudi, P. Moamaei, and R. Ahmadi, "A new fault-tolerant strategy based on a modified selective harmonic technique for three-phase multilevel converters with a single faulty cell," *IEEE Trans. Power Electron.*, vol. 31, no. 4, pp. 3141–3150. Apr. 2016.
[18] M. Boby, S. Arun Rahul, K. Gopakumar, L. Umanand, F. Blaabjerg, and S. Bhattacharya, "A low-order harmonic elimination scheme for induction motor drives using a multilevel octadecagonal space vector structure with a single DC source," *IEEE Trans. Power Electron.*, vol. 33, no. 3,. pp. 2430–2437. Mar. 2018.
[19] S. Mukherjee and G. Poddar, "A series-connected three-level inverter topology for medium-voltage squirrel-cage motor drive applications," *IEEE Trans. Ind. Appl.*, vol. 46, no. 1, pp. 179–186, Jan./Feb. 2010.
[20] B. Li, S. Zhou, and D. Xu, "A hybrid modular multi-level converter for medium-voltage variable-speed motor drives," *IEEE Trans. Power Electron.*, vol. 32, no. 6, pp. 4619–4630. Jun. 2017.
[21] K. Sivakumar, A. Das, R. Ramchand, C. Patel, and K. Gopakumar, "A hybrid multilevel inverter topology for an open-end winding induction-motor drive using two-level inverters in series with a capacitor-fed H-bridge cell," *IEEE Trans. Ind. Electron.*, vol. 57, no. 11, pp. 3707–3714, Nov. 2010.
[22] A. Edpuganti and A. K. Rathore, "Optimal low switching frequency pulse width modulation of nine-level cascade inverter," *IEEE Trans. Power Electron.*, vol. 30, no. 1, pp. 482–495, Jan. 2015.
[23] S. Fan, K. Zhang, J. Xiong, and Y. Xue, "An improved control system for modular multilevel converters with new modulation strategy and voltage balancing control," *IEEE Trans. Power Electron.*, vol. 30, no. 1, pp. 358–371, Jan. 2015.
[24] B. Tai, C. Gao, X. Liu, and Z. Chen, "A novel flexible capacitor voltage control strategy for variable-speed drives with modular multilevel converters," *IEEE Trans. Power Electron.*, vol. 32, no. 1, pp. 128–141, Jan 2017.
[25] K. Tian, B. Wu, M. Narimani, D. (D.) Xu, Z. Cheng, and N. R. Zargari, "A capacitor voltage-balancing method for nested neutral point clamped (NNPC) inverter," *IEEE Trans. Power Electron.*, vol. 31, no. 3, pp. 2575–2583, Mar. 2016.
[26] A. Antonopoulos, L. Angquist, L. Harnefors, and H.-P. Nee, "Optimal selection of the average capacitor voltage for variable-speed drives with modular multi level converters," *IEEE Trans. Power Electron.*, vol. 30, no. 1, pp. 227–234, Jan. 2015.
[27] S.-H. Ryu, D.-H. Kim, M.-J. Kim, J.-S. Kim, and B.-K. Lee, "Adjustable frequency–duty-cycle hybrid control strategy for full-bridge series resonant converters in electric vehicle chargers," *IEEE Trans. Ind. Electron.*, vol. 61, no. 10, pp. 5354–5362, Oct. 2014.
[28] D. S. Gautam, F. Musavi, W. Eberle, and W. G. Dunford, "A zero-voltage switching full-bridge dc-dc converter with capacitive output filter for plug-in hybrid electric vehicle battery charging," *IEEE Trans. Power Electron.*, vol. 28, no. 12, pp. 5728–5735, Dec. 2013.
[29] G. Liu, Y. Jang, M. M. Jovanović, and J. Q. Zhang, "Implementation of a 3.3-kW DC–DC converter for EV on-board charger employing the series-resonant converter with reduced-frequency-range control," *IEEE Trans. Power Electron.*, vol. 32, no. 6, pp. 4168–4184, Jun. 2017.
[30] N. S. González-Santini, H. Zeng, Y. Yu, and F. Z. Peng, "Z-Source resonant converter with power factor correction for wireless power transfer applications," *IEEE Trans. Power Electron.*, vol. 31, no. 11, pp. 7691–7700, Nov. 2016.
[31] R. Beiranvand, B. Rashidian, M. R. Zolghadri, and S. M. H. Alavi, "A design procedure for optimizing the LLC resonant converter as a wide output range voltage source," *IEEE Trans. Power Electron.*, vol. 27, no. 8, pp. 3749–3763, Aug. 2012.
[32] H. Hu, X. Fang, F. Chen, Z. J. Shen, and I. Batarseh, "A modified high efficiency LLC converter with two transformers for wide input-voltage range applications," *IEEE Trans. Power Electron.*, vol. 28, no. 4, pp. 1946–1960, Apr. 2013.
[33] E. H. Kim and B. H. Kwon, "Zero-voltage- and zero-current-switching full-bridge converter with secondary resonance," *IEEE Trans. Ind. Electron.*, vol. 57, no. 3, pp. 1017–1025, Mar. 2010.
[34] C. Liu *et al.*, "High-efficiency hybrid full-bridge–half-bridge converter with shared ZVS lagging leg and dual outputs in series," *IEEE Trans. Power Electron.*, vol. 28, no. 2, pp. 849–861, Feb. 2013.
[35] H. S. Kim, J. H. Jung, J. W. Baek, and H. J. Kim, "Analysis and design of multi-output converter using asymmetrical PWM half-bridge fly back converter employing a parallel-series transformer," *IEEE Trans. Ind. Electron.*, vol. 60, no. 8, pp. 3115–3125, Aug. 2013.

Sharifaddin Sharif was born in Kazerun, Iran. He received the M.S. degree in electronic engineering from Shiraz University, Shiraz, Iran.

He has been a Faculty Member with the Department of Electrical Engineering, the Islamic Azad University, Kazerun, Iran, since 1993. His research interest includes adjustable-speed motor drives, ac stabilizers, and photovoltaic grid-connected inverters.